SIMULATION ON NATURAL CONVECTION OF CARREAU FLUIDS IN A LOCALLY HEATED TRAPEZOIDAL CAVITY

***Shuguang LI*[1,*]*, Zhuoran ZHUANG*[1]*, Xiaoyi MA*[1]

[1]School of Science, Dalian Maritime University, Dalian, Liaoning116026, China

[*]Corresponding author ; E-mail : shuguangli2008@126.com

The laminar natural convection of non-Newtonian Carreau fluids in a trapezoidal cavity with a local heat source at the bottom is numerically investigated. A stabilized streamline–upwind/Petrov–Galerkin (SUPG) finite element algorithm is proposed, in which equal low-order finite elements are used. Effects of Rayleigh number (i.e., $Ra = 10^4$ and 10^5), power-law index (i.e., $0.6 \leq n \leq 1.4$), Prandtl number (i.e., $0.1 \leq Pr \leq 100$), and local heat source length (i.e., $0.1 \leq \eta \leq 1.0$) are researched. Results show that for different power-law indexes, as Prandtl numbers increase, the convective heat transfer is enhanced ; as power-law indexes increase, influences of Prandtl numbers decrease, as local heat source length increase, the convective heat transfer is enhanced.

Keywords : *Stabilized finite element ; Carreau fluids ; Natural convection ; Trapezoidal cavity ; Local heat source*

1 Introduction

Natural convection in cavities with complex geometric shapes is widely used in cooling of electronic equipment, solar collectors, cooling of nuclear reactors, etc., see [1] for futher details. In the past, a large number of studies focused on this type of natural convection for Newtonian fluids [2, 3]. In most of the above industrial applications, the flow usually exhibits a certain non-Newtonian viscosity [4, 5]. Therefore, natural convection of non-Newtonian fluids in trapezoidal cavities with local heat sources is a very interesting topic.

Generalized Newtonian fluids with shear rate dependence are an important part of rheology, and a large number of constitutive models have been developed, including the power-law model, the Carreau model, etc., see [6] for futher details. In recent studies, the effect of non-Newtonian viscosity on natural convection has been noted [7, 8]. The influence of parameters of Carreau–Yasuda constitutive equation on natural convection in a rectangular cavity is discussed in [9]. In [10], the laminar natural convection of power-law fluids in 2D trapezoidal enclosure with a heated bottom wall is analyzed.

A large amount of work has shown that numerical simulation has become an important tool for natural convection problems, including finite difference method [8, 9, 11, 12], finite volume method [10], finite element method [13] and lattice Boltzmann method [7]. The solution of natural convection problems by finite element method requires a stabilization method to avoid spurious oscillations caused by the nonlinear convection term. Many stabilized formulas based on the finite element method have been developed, such

as SUPG [14], Galerkin/least–squares (GLS) [15], and other methods [16]. It is worth mentioning that although various methods have been proposed to solve non-Newtonian problems [17], there is still a need for numerical methods that can achieve equal low-order finite elements $[18-20]$. This paper adopts a stabilized algorithm to study the natural convection of Carreau fluids in a trapezoidal cavity with a local heat source. By using the penalty function method to solve the velocity-pressure coupling term and the SUPG formulation to solve the momentum equation and energy equation containing nonlinear convection terms, and the numerical stability of the equal low-order elements can be guaranteed.

The rest of this paper is organized as follows. In Section 2, the mathematical model for natural convection of Carreau fluids in an isosceles trapezoidal cavity with a local heat source is proposed. In Section 3, a stabilized SUPG algorithm based on a penalty function is proposed. In Section 4, effects of Prandtl numbers and local heat source lengths on the natural convection of Carreau fluids are analyzed.

2 Governing equations

2.1 Problem description and governing equations

The model is shown in Fig. 1. The length and height of the lower base of the isosceles trapezoidal cavity are both L, and the left and right walls maintain a constant angle $\varphi = \pi/6$ with the vertical direction. The left and right inclined walls of the cavity maintain a constant low temperature T_{c}, and the bottom wall has a heat source with a length of $0 < L_{\mathrm{h}} \leq L$ and a constant high temperature T_{h}, and the rest of the wall is insulated. The cavity is filled with Carreau fluids. The natural convection satisfies : (1) The flow is incompressible and laminar, and meets the no-slip boundary condition ; (2) The flow is in local thermal equilibrium with no heat generation, no thermal radiation, no viscous dissipation and no chemical reaction ; (3) The density variation with temperature is described by the Boussinesq approximation : $\bar{\rho} = \rho_0[1 - \beta(\bar{T} - T_{\mathrm{c}})]$, where β is the thermal expansion coefficients, ρ is the density, ρ_0 is the initial density and $\bar{T}$ is the temperature.

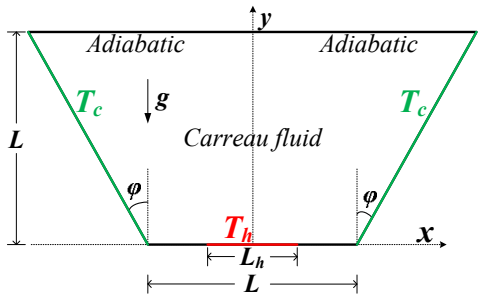

Fig. 1. Geometry of the present study.

The governing equations for natural convection of Carreau fluids are as follows [7] :

$$\nabla \cdot \bar{\mathbf{v}} = 0, \tag{1}$$

$$\rho_0 \bar{\mathbf{v}} \cdot \nabla \bar{\mathbf{v}} = -\nabla \bar{p} + \nabla \cdot \bar{\tau} + \bar{\rho}\mathbf{g}, \tag{2}$$

$$\bar{\tau} = 2\bar{\mu}\bar{\varepsilon},\ \bar{\varepsilon} = \frac{1}{2}(\nabla \bar{\mathbf{v}} + \nabla \bar{\mathbf{v}}^T),\ \frac{\bar{\mu} - \mu_\infty}{\mu_0 - \mu_\infty} = \left[1 + (\lambda \mathbf{I}_2)^2\right]^{\frac{n-1}{2}},\ \mathbf{I}_2 = \sqrt{2\bar{\varepsilon} : \bar{\varepsilon}}, \tag{3}$$

$$\bar{\mathbf{v}} \cdot \nabla \bar{T} = \alpha \nabla^2 \bar{T}, \tag{4}$$

where $\bar{\mathbf{v}} = (\bar{u}, \bar{v})$ is the velocity field, $\bar{p}$ is the pressure, $\mathbf{g}$ is the mass force, α is the thermal diffusion coefficient, $\bar{\tau}$ is the viscous stress tensor, $\bar{\varepsilon}$ is the deformation rate tensor, $\bar{\mu}$ is the viscosity, μ_0 and μ_∞ are the viscosities corresponding to zero- and infinite-shear-rate viscosities, λ is a time constant, n is the power-law index, and $\mathbf{I}_2$ is the shear rate or the equivalent strain rate.

The boundary $\bar{\Gamma} = \partial\bar{\Omega}$ is the boundary of the flow area $\bar{\Omega}$, which consists of four disjoint subsets :

$$\bar{\Gamma}_1 = \{(\bar{x}, \bar{y}) : -\frac{L_\mathrm{h}}{2} \le \bar{x} \le \frac{L_\mathrm{h}}{2}, \bar{y} = 0\}, \bar{\Gamma}_2 = \{(\bar{x}, \bar{y}) : -\frac{L}{2} - L\tan\varphi \le \bar{x} \le \frac{L}{2} + L\tan\varphi, \bar{y} = L\},$$
$$\bar{\Gamma}_3 = \{(\bar{x}, \bar{y}) : \frac{L_\mathrm{h}}{2} \le \bar{x} \le \frac{L}{2}, \bar{y} = 0\} \cup \{(\bar{x}, \bar{y}) : -\frac{L}{2} \le \bar{x} \le -\frac{L_\mathrm{h}}{2}, \bar{y} = 0\},$$
$$\bar{\Gamma}_4 = \{(\bar{x}, \bar{y}) : \frac{L}{2} \le \bar{x} \le \frac{L}{2} + L\tan\varphi, \bar{y} = \frac{\bar{x} - \frac{L}{2}}{\tan\varphi}\} \cup \{(\bar{x}, \bar{y}) : -\frac{L}{2} - L\tan\varphi \le \bar{x} \le -\frac{L}{2}, \bar{y} = \frac{\bar{x} + \frac{L}{2}}{\tan\varphi}\}.$$

The boundary conditions of the problem are as follows :

$$\bar{\mathbf{v}}|_{\bar{\Gamma}_1} = 0, \quad \bar{T}|_{\bar{\Gamma}_1} = T_\mathrm{h}, \qquad \bar{\mathbf{v}}|_{\bar{\Gamma}_2 \cup \bar{\Gamma}_3} = 0, \quad \frac{\partial \bar{T}}{\partial \mathbf{n}}|_{\bar{\Gamma}_2 \cup \bar{\Gamma}_3} = 0, \qquad \bar{\mathbf{v}}|_{\bar{\Gamma}_4} = 0, \quad \bar{T}|_{\bar{\Gamma}_4} = T_\mathrm{c}.$$

2.2 Non-dimensional equations

The non-dimensional variables are introduced for equations $(1) - (4)$, as follows :

$$(x, y) = \frac{(\bar{x}, \bar{y})}{L},\ \mathbf{v} = (u, v) = \frac{(\bar{u}, \bar{v})L}{\alpha},\ p = \frac{L^2\bar{p}}{\rho_0\alpha^2},\ T = \frac{\bar{T} - T_\mathrm{c}}{T_\mathrm{h} - T_\mathrm{c}},\ \mu = \frac{\bar{\mu}}{\mu_0}. \tag{5}$$

By substituting equation (5) into equations $(1) - (4)$, the non-dimensional equations are obtained :

$$\nabla \cdot \mathbf{v} = 0, \tag{6}$$
$$\mathbf{v} \cdot \nabla\mathbf{v} = -\nabla p + Pr\nabla \cdot \tau + RaPr\delta_{i,2}T, \tag{7}$$
$$\tau = 2\mu\varepsilon,\ \varepsilon = \frac{1}{2}(\nabla\mathbf{v} + \nabla\mathbf{v}^T),\ \mu = s + (1 - s)[1 + (Cu\sqrt{2\varepsilon : \varepsilon})^2]^{\frac{n-1}{2}}, \tag{8}$$
$$\mathbf{v} \cdot \nabla T = \nabla^2 T, \tag{9}$$

where $s = \dfrac{\mu_\infty}{\mu_0}$ is the ratio of infinite shear rate to zero shear rate viscosity, $Cu = \dfrac{\lambda\alpha}{L^2}$ is Carreau number, $Ra = \dfrac{\rho_0 g L^3 \beta(T_h - T_c)}{\mu_0\alpha}$ is Rayleigh number, $Pr = \dfrac{\mu_0}{\rho_0\alpha}$ is Prandtl number. Here $s = 10^{-4}$.

$\Gamma = \partial\Omega$ is the boundary of the non-dimensional area Ω, and $0 \le \eta = \frac{L_\mathrm{h}}{L} \le 1$ is the non-dimensional local heat source length :

$$\Gamma_1 = \{(x, y) : -\frac{\eta}{2} \le x \le \frac{\eta}{2}, y = 0\}, \qquad \Gamma_2 = \{(x, y) : -\frac{1}{2} - \tan\varphi \le x \le \frac{1}{2} + \tan\varphi, y = 1\},$$
$$\Gamma_3 = \{(x, y) : \frac{\eta}{2} \le x \le \frac{1}{2}, y = 0\} \cup \{(x, y) : -\frac{1}{2} \le x \le -\frac{\eta}{2}, y = 0\},$$
$$\Gamma_4 = \{(x, y) : \frac{1}{2} \le x \le \frac{1}{2} + \tan\varphi, y = \frac{x - \frac{1}{2}}{\tan\varphi}\} \cup \{(x, y) : -\frac{1}{2} - \tan\varphi \le x \le -\frac{1}{2}, y = \frac{x + \frac{1}{2}}{\tan\varphi}\}.$$

The non-dimensional expression of the boundary conditions is as follows :

$$\mathbf{v}|_{\Gamma_1} = 0, \quad T|_{\Gamma_1} = 1, \qquad \mathbf{v}|_{\Gamma_2 \cup \Gamma_3} = 0, \quad \frac{\partial T}{\partial \mathbf{n}}|_{\Gamma_2 \cup \Gamma_3} = 0, \qquad \mathbf{v}|_{\Gamma_4} = 0, \quad T|_{\Gamma_4} = 0.$$

The local Nusselt number $Nu(x)$ and average Nusselt number Nu_0 on the hot wall are defined as : $Nu(x) = -\dfrac{\partial T}{\partial \mathbf{n}}$ and $Nu_0 = \dfrac{1}{\eta}\displaystyle\int_{-\frac{\eta}{2}}^{\frac{\eta}{2}} Nu(x)dx$, where $\mathbf{n}$ is the normal direction on the wall. The average viscosity is introduced in this work to describe non-Newtonian behavior : $\mu_{\text{avg}} = \displaystyle\int_{\Omega} \mu(x,y)d\Omega$, where Ω is the region of the considered trapezoidal cavity.

3 Numerical methods

In this section, a SUPG stabilized algorithm based on a penalty function is proposed to solve the system $(6)-(9)$, which can use equal low-order elements of velocity, pressure and temperature.

3.1 SUPG finite element formulation based on penalty function

The penalty factor γ is introduced into equation (6), so that following equation holds true $[20, 21]$:

$$p = -\gamma(\nabla \cdot \mathbf{v}), \tag{10}$$

where the γ value is large enough and in this work $\gamma = 10^7$.

The finite-dimensional solution and test function spaces are defined as follows $[18, 22]$:

$$\mathcal{S}_{\mathbf{v}}^h = \left\{\mathbf{v}^h : \mathbf{v}^h \in \left[\mathcal{H}_1^h(\Omega)\right]^{n_{sd}}, \mathbf{v}^h = \mathbf{v}^D \; on \; \Gamma^D\right\}, \mathcal{S}_T^h = \left\{T^h : T^h \in \left[\mathcal{H}_1^h(\Omega)\right], T^h = T^D \; on \; \Gamma^D\right\},$$
$$\mathcal{V}_{\mathbf{v}}^h = \left\{\mathbf{w}^h : \mathbf{w}^h \in \left[\mathcal{H}_1^h(\Omega)\right]^{n_{sd}}, \mathbf{w}^h = 0 \; on \; \Gamma^D\right\}, \mathcal{V}_T^h = \left\{T^h : T^h \in \left[\mathcal{H}_1^h(\Omega)\right], T^h = 0 \; on \; \Gamma^D\right\},$$

where $\mathbf{v}^D$ and T^D are the Dirichlet-type boundary conditions associated with the velocity $\mathbf{v}$ and the temperature T, and n_{sd} represents the spatial dimension ($n_{\text{sd}} = 2$ in this paper).

By introducing the SUPG stabilization term and equation (10), the stabilization formula of system $(6)-(9)$ can be obtained (for all $\mathbf{w}^h \in \mathcal{V}_{\mathbf{v}}^h$ and $w^h \in \mathcal{V}_T^h$, find $\mathbf{v}^h \in \mathcal{S}_{\mathbf{v}}^h$ and $T^h \in \mathcal{S}_T^h$ so that the following equation holds) as follows $[18, 22]$:

$$\begin{aligned}\int_{\Omega} \mathbf{w}^h(\mathbf{v}^h \cdot \nabla \mathbf{v}^h - RaPr\mathbf{f}^h)d\Omega + Pr\int_{\Omega} \mu^h(\nabla \mathbf{w}^h)\cdot(\nabla \mathbf{v}^h)d\Omega + \gamma\int_{\Omega}(\nabla\cdot\mathbf{w}^h)(\nabla\cdot\mathbf{v}^h)d\Omega \\ + \int_{\Omega} w^h(\mathbf{v}^h\cdot\nabla T^h)d\Omega + \int_{\Omega}(\nabla w^h)\cdot(\nabla T^h)d\Omega - \int_{\Gamma_h}\mathbf{w}^h\mathbf{h}^h d\Gamma - \int_{(\Gamma_h)_T} w^h h^h d\Gamma \\ + \sum_{e=1}^{n_{\text{ele}}}\int_{\Omega^e}(\gamma_{\text{supg}}\mathbf{v}^h\cdot\nabla\mathbf{w}^h)\cdot\mathbf{r}_{\mathbf{v}}^h d\Omega + \sum_{e=1}^{n_{\text{ele}}}\int_{\Omega^e}(\gamma_{\text{supg}}\mathbf{v}^h\cdot\nabla\mathbf{w}^h)\cdot\mathbf{r}_T^h d\Omega = 0,\end{aligned} \tag{11}$$

where the discrete functions with superscript $'h'$ represent from the finite-dimensional space. $\mathbf{h}^h$ and h^h represent the Neumann boundary conditions of velocity and temperature, Γ_h and $(\Gamma_h)_T$ are the corresponding Neumann boundaries. n_{ele} is the number of elements, and e is the element counter. The residual vectors $\mathbf{r}_{\mathbf{v}}^h$ and $\mathbf{r}_T^h$ associated with the momentum equation and energy equation are defined as :

$$\mathbf{r}_{\mathbf{v}}^h = \mathbf{v}^h\cdot\nabla\mathbf{v}^h - Pr\nabla\cdot[\mu^h(\nabla\mathbf{v}+\nabla\mathbf{v}^T)] - \gamma\nabla(\nabla\cdot\mathbf{v}^h) - RaPr\mathbf{f}^h$$
$$\mathbf{r}_T^h = \mathbf{v}^h\cdot\nabla T^h - \nabla\cdot(\nabla T^h).$$

The stabilization parameter γ_{supg} is defined as [20, 23] :

$$\gamma_{\text{supg}} = \frac{h^e}{2\|\mathbf{v}^e\|} \frac{1}{\sqrt{1 + 6\nu/(\|\mathbf{v}^e\| h^e)}},$$

where $h^e = \sqrt{A_e}$ is the characteristic element size, A_e is the element area in two dimensions, $\mathbf{v}^e$ is the convection velocity in the element center of mass, the average of velocities at each node in the element, and $\|\cdot\|$ is the standard Euclidean norm, and ν is the kinematic viscosity.

3.2 Code validation and grid independence

The linear equal low-order elements of velocity-pressure-temperature are used in this work. The benchmark solution of the natural convection for the Newtonian fluid ($n = 1.0$) in a square cavity is solved to verify the accuracy and effectiveness of the numerical method, and the results are listed in Tab. 1.

Table 1. Comparison of benchmark solutions by different numerical methods for the Newtonian fluid in a square cavity at $Pr = 0.71$ when $Ra = 10^4$ and 10^5

Ra	Mesh	$\lvert\psi_{\text{mid}}\rvert$	$\lvert\psi\rvert_{\max}$	$u_{\max}$	$v_{\max}$	Nu_0	$Nu_{\max}$	$Nu_{\min}$
10^4	Present (100×100)	5.0732	5.0732	16.1970	19.6466	2.2405	3.5751	0.5851
	Ref.[24] (129×129)	5.0741	5.0741	16.1817	19.6284	2.2449	3.5313	0.5850
	Ref.[25] (81×81)	5.0738	5.0738	16.1837	19.6282	2.2441	3.5295	0.5847
10^5	Present (100×100)	9.1097	9.6294	34.7889	68.5969	4.5051	7.6614	0.7285
	Ref.[24] (129×129)	9.1194	9.6202	34.7363	68.5385	4.5214	7.7216	0.7280
	Ref.[25] (81×81)	9.1161	9.6173	34.7417	68.6383	4.5195	7.7121	0.7275

The variables listed here are : the absolute value of streamfunction $|\psi_{\text{mid}}|$ at the midpoint of the cavity, the maximum absolute value of streamfunction $|\psi|_{\max}$, the maximum horizontal velocity $u_{\max}$ on the vertical midplane, the maximum vertical velocity $v_{\max}$ on the horizontal midplane, the average Nusselt number Nu_0 on the hot wall, and the maximum and minimum values $Nu_{\max}$ and $Nu_{\min}$ of the local Nusselt number on the hot wall. Tab. 1 shows that the benchmark solution obtained by the proposed numerical method is highly consistent with the results of the high-precision compact methods in [24] and [25].

Table 2. Grid independence study of the shear-thinning fluid ($n = 0.6, Cu = 2$) in the trapezoidal cavity($\eta = 0.5$) at $Pr = 10$ when $Ra = 10^4$ and 10^5

	$Ra = 10^4$				$Ra = 10^5$			
Mesh	μ_{avg}	$\lvert\psi\rvert_{\max}$	$v_{\max}$	Nu_0	μ_{avg}	$\lvert\psi\rvert_{\max}$	$v_{\max}$	Nu_0
(80×80)	0.7200	6.2562	33.9790	3.0311	0.6935	21.9424	170.0062	5.7385
(92×92)	0.7204	6.2554	34.0219	3.0650	0.6944	21.9771	170.8303	5.8146
(100×100)	0.7206	6.2599	34.0421	3.0836	0.6949	21.9942	171.2502	5.8558
(112×112)	0.7209	6.2589	34.0651	3.1073	0.6954	22.0084	171.7464	5.9070

Next, natural convection of shear-thinning fluid ($n = 0.6, Cu = 2$) is performed in a trapezoidal cavity with a local heat source. The numerical results are shown in Tab. 2, and the difference between the numerical results of grid 100×100 and the results of grids with higher density is less than 0.5%.

4 Results and discussion

The results in $[7-9, 12]$ show that in natural convection of generalized Newtonian fluids at different Rayleigh numbers, the flow and heat transfer are weakened with increasing power-law index. Here, natural convection of Carreau fluids in a trapezoidal cavity with a local heat source at the bottom is focused on.

4.1 Effects of Prandtl numbers on flow and heat transfer

In this subsection, the effects of Prandtl numbers on the natural convection of Carreau fluids in an isosceles trapezoidal cavity with a local heat source of $\eta = 0.5$ at the bottom is investigated.

Fig. 2 illustrates the streamlines for different power-law indexes n and Prandtl numbers Pr at $Ra = 10^5$. Fig. 2 shows that streamlines is basically symmetrical about the central axis of the cavity, and for different n, the value of streamlines increases significantly with the increase of Pr. For a fixed Pr, the value of streamlines decreases with the increase of n. With the increase of Pr, the streamlines value at the vortex core gradually increases from 13 to 22 for $n = 0.6$; from 11 to 15 for $n = 1.0$; and from 10 to 12 for $n = 1.4$. It shows that the influence of Pr on streamlines weakens with the increase of n.

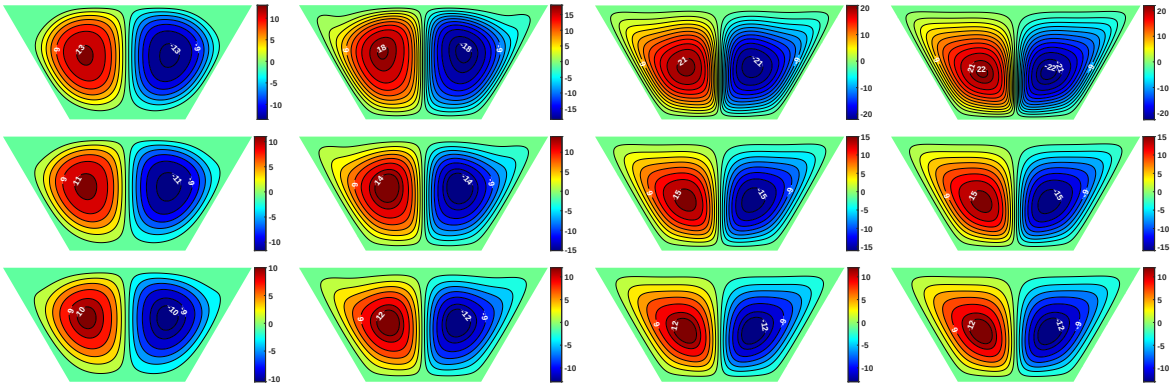

Fig. 2. Streamlines of Carreau fluids natural convection with different Prandtl numbers Pr and power-law indexes n in a trapezoidal cavity with a heat source of $\eta = 0.5$ at $Ra = 10^5$: from top to bottom $n = 0.6$, 1.0, 1.4 and from left to right : $Pr = 0.1$, 1.0, 10, 100.

Fig. 3 shows the isotherms for different power-law indexes n and Prandtl numbers Pr at $Ra = 10^5$. Fig. 3 shows that isotherms is basically symmetrical about the central axis of the cavity, and for different n, the temperature gradient at the local heat source increases with the increase of Pr, which is particularly obvious for $n = 0.6$. For a fixed Pr, the temperature gradient at the local heat source decreases with the increase of n. It is clearly observed that at $n = 0.6$, the distribution of isotherms in the cavity shows obvious differences with the increase of Pr, especially for isotherms with values of 0.3 and 0.4, but when $n = 1.0$ and $n = 1.4$, the difference in isotherms at different Pr weakens. It shows that at $Ra = 10^5$, with the increase of n, the influence of Pr on isotherms weakens.

Furthermore, local Nusselt number $Nu(x)$ on the local heat source and velocity $v(x)$ in the middle of the cavity for different power-law indexes n and Prandtl numbers Pr are indicated in Fig. 4. Fig. 4 shows that for different n, $Nu(x)$ and $v(x)$ increase with the increase of Pr. Fig. 4 shows that at $Pr = 10$, the

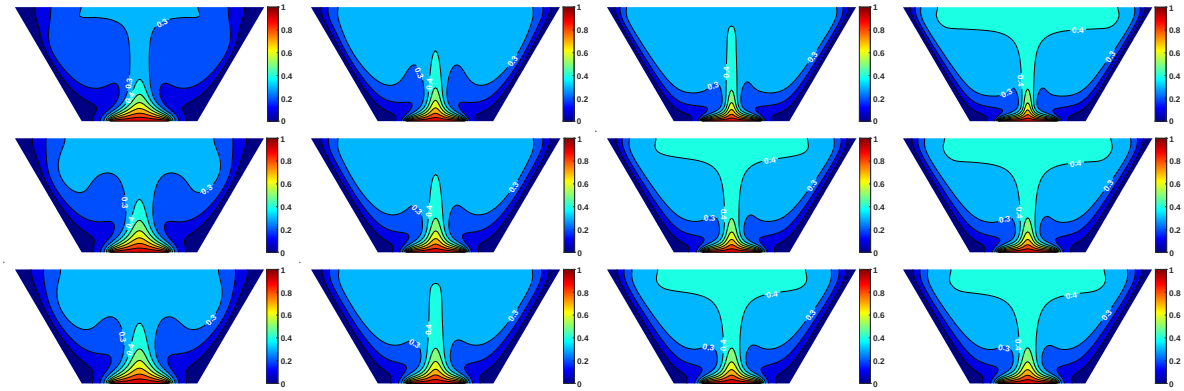

Fig. 3. Isotherms of Carreau fluids natural convection with different Prandtl numbers Pr and power-law indexes n in a trapezoidal cavity with a heat source of $\eta = 0.5$ at $Ra = 10^5$: from top to bottom $n = 0.6$, 1.0, 1.4 and from left to right : $Pr = 0.1$, 1.0, 10, 100.

influence of n on the $Nu(x)$ and the $v(x)$ velocity in the middle of the cavity is significantly stronger than that at $Pr = 0.1$ and $Pr = 0.71$. Fig. 4 shows that the influence of n increase with the increase of Pr.

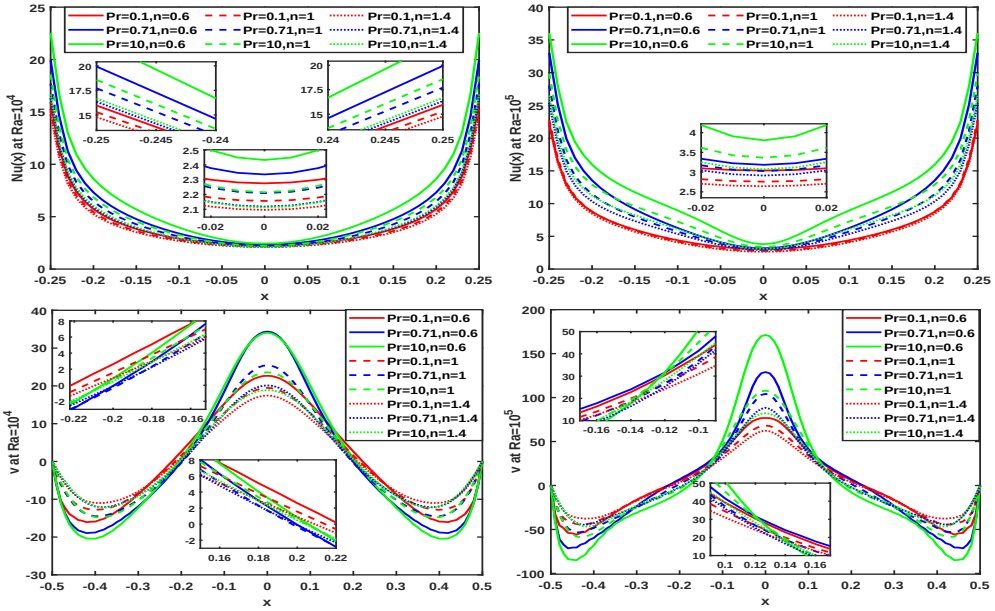

Fig. 4. Comparisons of local Nusselt number $Nu(x)$ on the local heat source and v velocity distributions at $y = 0.5$ for different Prandtl numbers Pr and power-law indexes n at $Ra = 10^4$(left) and 10^5 (right).

Fig. 5 indicates the variation of average viscosities μ_{avg}, average Nusselt numbers Nu_0 and the maximum absolute value of streamfunctions $|\psi|_{\max}$ with different Prandtl numbers Pr for different power-law indexes n when $Ra = 10^4$ and 10^5, respectively. Obviously, influences of n and Pr are significantly stronger when $Ra = 10^5$ than when $Ra = 10^4$. As shown in Fig. 5, for different n, as Pr increase, Nu_0 gradually increases, and $|\psi|_{\max}$ first increase and then tend to be flat. Fig. 5 shows that the effect of Pr weaken with the increase of n. Tab. 3 gives the quantitative results of numerical simulation. Tab. 3 shows that for different n, as Pr increase, Nu_0 and $|\psi|_{\max}$ show large differences. For example, when $Ra = 10^5$, growth rates of Nu_0 for $n = 0.6$ is 45.94%, 3.56%, 19.24%, and 7.24%, for $n = 1.0$ is 28.98%, 2.82%, 12.45%, and 1.98%, and

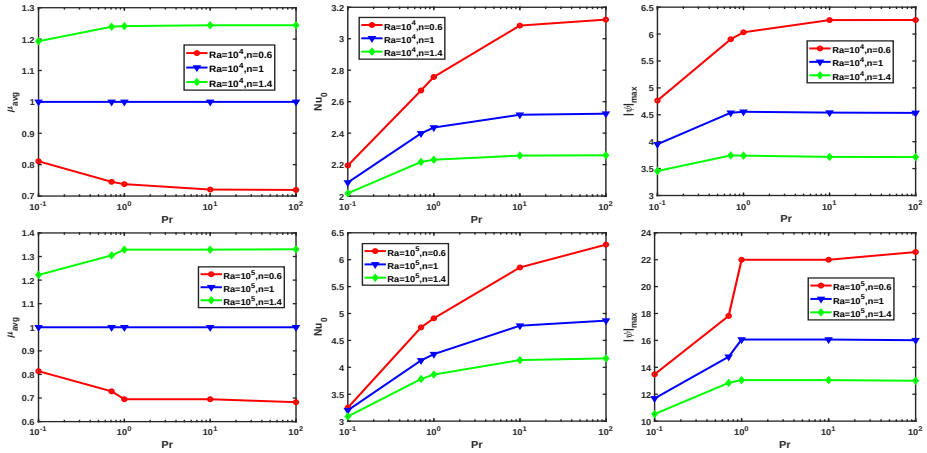

Fig. 5. The effect of Prandtl numbers Pr on the average viscosity μ_{avg}, the average Nusselt number Nu_0 on the hot wall and the maximum streamfunction $|\psi|_{\max}$ for different power-law indexes n in a trapezoidal cavity with a heat source of $\eta = 0.5$ at $Ra = 10^4$ (top) and $Ra = 10^5$ (bottom).

for $n = 1.4$ is 22.57%, 2.19%, 6.95%, and 0.77%. Interestingly, when $Ra = 10^5$, growth rates of $|\psi|_{\max}$ for $n = 0.6$ is 32.19%, 3.33%, 19.45%, and 2.61%, for $n = 1.0$ is 26.50%, 2.84%, 5.66%, and -0.32%, for $n = 1.4$ is 22.03%, 1.50%, 0.10%, and -0.35%. Tab. 3 shows that the influence of Pr decreases with the increase of n.

Table 3. Comparisons of numerical results for different Rayleigh numbers, power-law indexes and Prandtl numbers in a trapezoidal cavity with a heat source length of $\eta = 0.5$.

		$Ra = 10^4$					$Ra = 10^5$				
	Pr	0.1	0.71	1	10	100	0.1	0.71	1	10	100
$n = 0.6$	μ_{avg}	0.8107	0.7453	0.7379	0.7206	0.7195	0.8139	0.7284	0.7204	0.6949	0.6824
	Nu_0	2.1941	2.6712	2.7572	3.0836	3.1217	3.2494	4.7421	4.9110	5.8558	6.2800
	$\|\psi\|_{\max}$	4.7643	5.9033	6.0328	6.2599	6.2617	13.4800	17.8188	18.4127	21.9942	22.5680
$n = 1.0$	μ_{avg}	1.0	1.0	1.0	1.0	1.0	1.0	1.0	1.0	1.0	1.0
	Nu_0	2.0861	2.3983	2.4356	2.5169	2.5235	3.2006	4.1282	4.2446	4.7732	4.8676
	$\|\psi\|_{\max}$	3.9528	4.5374	4.5556	4.5404	4.5349	11.6873	14.7846	15.2042	16.0648	16.0141
$n = 1.4$	μ_{avg}	1.1933	1.2394	1.2414	1.2441	1.2443	1.2219	1.3048	1.3122	1.3292	1.3308
	Nu_0	2.0176	2.2170	2.2311	2.2573	2.2592	3.0859	3.7825	3.8655	4.1342	4.1660
	$\|\psi\|_{\max}$	3.4548	3.7442	3.7405	3.7173	3.7145	10.5243	12.8427	13.0350	13.0482	13.0021

4.2 Effects of local heat source lengths on flow and heat transfer

In this subsection, the effect of the local heat source length η on the bottom edge of the trapezoidal cavity on the natural convection is further considered.

Fig. 6 exhibits streamlines with different local heat source lengths η and power-law indexes n when $Ra = 10^5$ and $Pr = 10$. Fig. 6 shows that streamlines are basically symmetrical about the central axis of the cavity, and for different n, the streamlines value increases significantly with the increase of η. For a fixed η, the streamlines value decreases with the increase of n. Interestingly, as η increases from 0.3 to 1.0, the

streamlines value at the vortex core gradually increases from 18 to 25 for $n = 0.6$; from 13 to 18 for $n = 1.0$ and from 11 to 14 for $n = 1.4$. This shows that as n increases, the effect of η on the streamlines decreases.

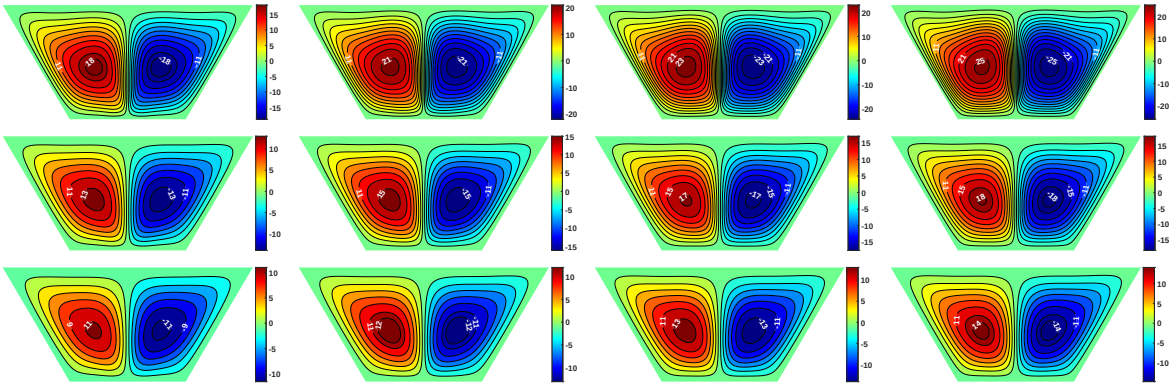

Fig. 6. Streamlines of Carreau fluids natural convection for different power-law indexes n in a trapezoidal cavity with different heat source lengths η at $Ra = 10^5$ and $Pr = 10$: from top to bottom $n = 0.6$, 1.0, 1.4 and from left to right : $\eta = 0.3$, 0.5, 0.7, 1.0.

Fig. 7 shows isotherms with different local heat source lengths η and power-law indexes n when $Ra = 10^5$ and $Pr = 10$. Fig. 7 shows that isotherms is basically symmetrical about the central axis of the cavity, and for different n, as the η increases, the temperature diffusion range in the cavity increases (such as the isotherms with values of 0.4 and 0.5), indicating that the heat transfer effect is enhanced.

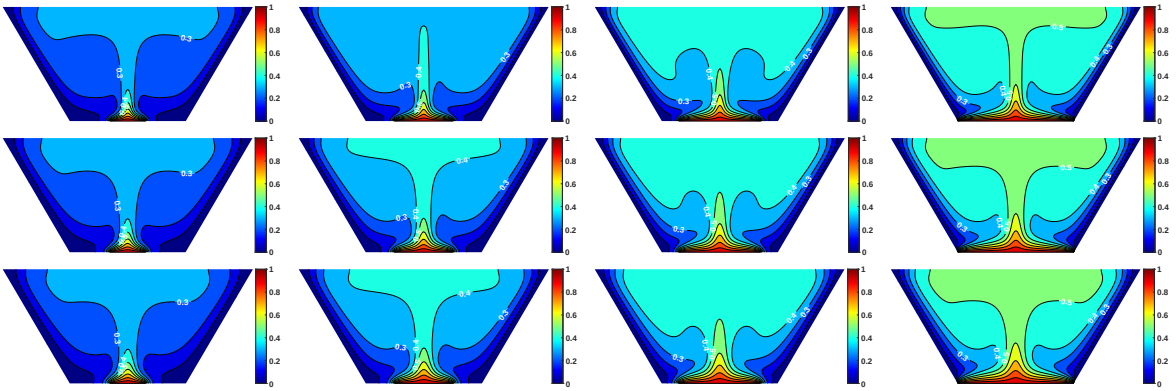

Fig. 7. Isotherms of Carreau fluid natural convection for different power-law indexes n in a trapezoidal cavity with different heat source lengths η at $Ra = 10^5$ and $Pr = 10$: from top to bottom $n = 0.6$, 1.0, 1.4 and from left to right : $\eta = 0.3$, 0.5, 0.7, 1.0.

Further, local Nusselt number $Nu(x)$ at the local heat source and the velocity $v(x)$ in the middle of the cavity for different power-law indexes n and local heat source lengths η at $Ra = 10^4$ and $Ra = 10^5$ are shown in Fig. 8. For different n, as the η increases, the $Nu(x)$ at the center of the bottom decreases, while the area enclosed by the $Nu(x)$ and the bottom increases. For different n, $v(x)$ increases with the increase of η. Fig. 8 shows that the effect of η on $Nu(x)$ and $v(x)$ is more significant at $Ra = 10^5$ than at $Ra = 10^4$.

Fig. 9 shows the variation of average viscosities μ_{avg}, average Nusselt numbers Nu_0 and the maximum absolute value of streamfunctions $|\psi|_{\max}$ with local heat source lengths η for different power-law indexes n when $Ra = 10^4$ and 10^5. Fig. 9 shows that with the increase of η, Nu_0 and $|\psi|_{\max}$ increase, and the

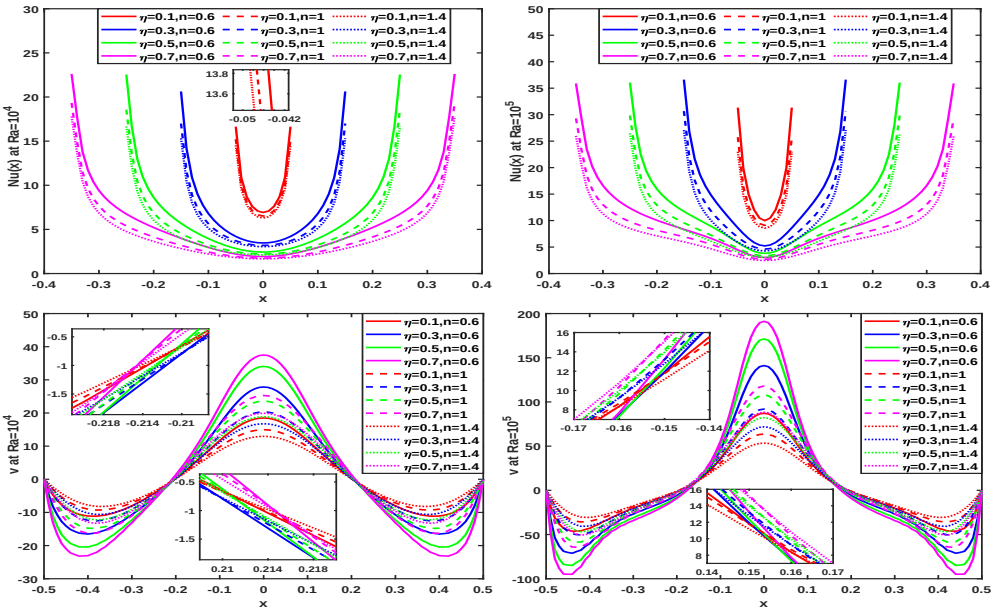

Fig. 8. Comparisons of local Nusselt number $Nu(x)$ on the hot wall and v velocity distributions at $y = 0.5$ with different heat source lengths η and power-law indexes n for a fixed Prandtl number $Pr = 10$ at $Ra = 10^4$(left) and 10^5 (right).

influence of n and η at $Ra = 10^5$ is significantly stronger than that at $Ra = 10^4$. From Fig. 9, it can be seen that for a fixed n, the trend of μ_{avg}, Nu_0 and $|\psi|_{\max}$ changing with the increase of η is more obvious at $Pr = 10$ than that at $Pr = 0.71$.

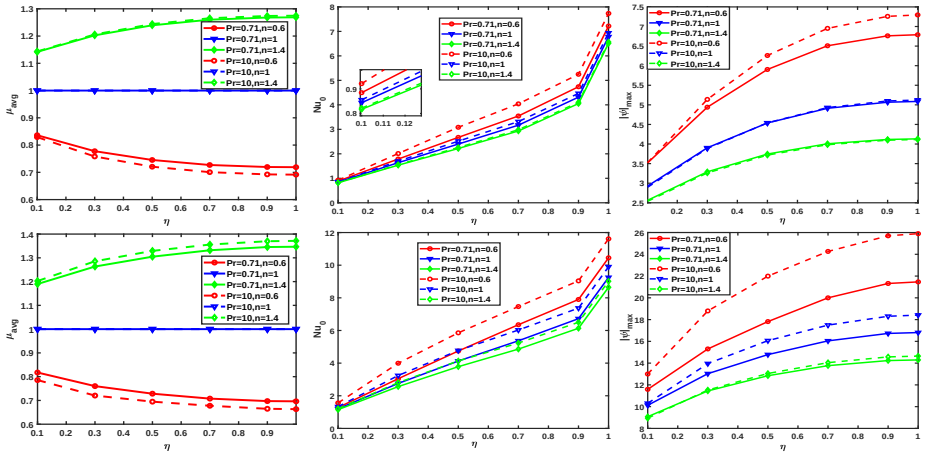

Fig. 9. The effect of heat source lengths η on the average viscosity μ_{avg}, the average Nusselt number Nu_0 on the hot wall and the maximum streamfunction $|\psi|_{\max}$ for different power-law indexes n and Prandtl numbers Pr at $Ra = 10^4$ (top) and $Ra = 10^5$ (bottom).

Tab. 4 gives the quantitative results of the numerical simulation, which shows that for different power-law indexes n, average Nusselt numbers Nu_0 and the maximum absolute value of streamfunctions $|\psi|_{\max}$ show different changes with the increase of local heat source lengths η. In particular, compared with the effect of η, the effects of n and Prandtl numbers Pr are very weak.

Table 4. Comparison of numerical results for different Rayleigh numbers and power-law indexes in a trapezoidal cavity with different heat source lengths η at $Pr = 10$.

		$Ra = 10^4$					$Ra = 10^5$				
	η	0.1	0.3	0.5	0.7	1.0	0.1	0.3	0.5	0.7	1.0
	μ_{avg}	0.8292	0.7582	0.7206	0.7006	0.6915	0.7856	0.7204	0.6949	0.6776	0.6633
$n = 0.6$	Nu_0	0.9213	2.0111	3.0836	4.0404	7.7344	1.5614	3.9932	5.8559	7.4656	11.6143
	$\lvert\psi\rvert_{\max}$	3.5153	5.1387	6.2599	6.9520	7.2958	12.9998	18.7960	21.9940	24.2652	25.8977
	μ_{avg}	1.0	1.0	1.0	1.0	1.0	1.0	1.0	1.0	1.0	1.0
$n = 1.0$	Nu_0	0.8554	1.6997	2.5169	3.3151	6.9372	1.3287	3.2415	4.7732	6.0276	9.9024
	$\lvert\psi\rvert_{\max}$	2.8903	3.8873	4.5404	4.9301	5.1226	10.3053	13.9566	16.0647	17.4935	18.4146
	μ_{avg}	1.1435	1.2059	1.2441	1.2654	1.2747	1.2024	1.2856	1.3292	1.3559	1.3715
$n = 1.4$	Nu_0	0.8218	1.5578	2.2573	2.9826	6.5665	1.2129	2.8057	4.1342	5.2312	9.0165
	$\lvert\psi\rvert_{\max}$	2.5331	3.2619	3.7173	3.9828	4.1154	8.9402	11.5271	13.0482	14.0438	14.6452

5 Conclusion

In this paper, a stabilized streamline–upwind/Petrov—Galerkin (SUPG) finite element algorithm based on a penalty function is proposed for natural convection of Carreau fluids in an isosceles trapezoidal cavity with a local heat source, which can realize equal low-order elements. The relevant parameters in the following ranges are studied : Rayleigh number $Ra = 10^4$ and 10^5, power-law index (i.e., $0.6 \leq n \leq 1.4$), Prandtl number $0.1 \leq Pr \leq 100$, and local heat source length at the bottom $0.1 \leq \eta \leq 1$.

Results show that when local heat source lengths are fixed, for different power-law indexes, as Prandtl numbers increases, average Nusselt numbers increase, indicating that the convective heat transfer is enhanced ; and as power-law indexes increase, influences of Prandtl numbers decrease. Results show that for different power-law indexes, as local heat source lengths increase, average Nusselt numbers and the maximum absolute value of streamfunction increase, indicating enhanced convective heat transfer. Results also show that as power-law indexes increase, effects of local heat source lengths decrease, but as Prandtl numbers increase, effects of local heat source lengths increase.

Acknowledgments

This work is supported by the "Fundamental Research Funds for the Central Universities in China" (No. 3132025204). The authors thank the anonymous reviewers for their valuable suggestions.

Nomenclature

Ra – Rayleigh number
β – Thermal expansion coefficients, [1/K]
α – Thermal diffusion coefficient, $[\mathrm{m^2 s^{-1}}]$
$\mathbf{I}_2$ – The equivalent of strain rate
μ – Viscosity
γ – Penalty factor
Pr – Prandtl number
ε – Deformation rate tensor
τ – Viscous stress tensor
ρ – Density, $[\mathrm{kgm^{-3}}]$
p – Dimensionless pressure
T – Dimensionless temperature
Cu – Carreau number
$\mathbf{g}$ – Mass force, $[\mathrm{m^2 s^{-1}}]$
ψ – Streamfunction
n – Power-law index
λ – A time constant
$\mathbf{v}$ – Velocity field

References

[1] Das, D., *et al.*, Studies on Natural Convection within Enclosures of Various (Non-Square) Shapes - a Review, *International Journal of Heat and Mass Transfer, 106* (2017), pp. 356-406

[2] Xia, Y. W., *et al.*, Direct Numerical Simulation of Double Diffusive Natural Convection in a Closed Mixture Cavity Heated from Below, *Thermal Science, 27* (2023), 5, pp. 4261-4275

[3] Mohebbi, R., *et al.*, Heat Source Location and Natural Convection in a C-Shaped Enclosure Saturated by a Nanofluid, *Physics of Fluids, 29* (2017), 12, pp. 122009

[4] Nouri, R., *et al.*, Non-Newtonian Natural-Convection in a Square Box Submitted to Horizontal Heat Flux and Magnetic Field, *Thermal Science, 28* (2024), 4A, pp. 3049-3061

[5] Horimek, A., Non-Newtonian Natural-Convection Cooling of a Heat Source of Variable Length and Position Placed at the Bottom of a Square Cavity, *Thermal Science, 27* (2023), 5B, pp. 4161-4178.

[6] Bird, R. B., *et al.*, Dynamics of polymeric liquids. volume 1 : Fluid mechanics, John Wiley, 1987

[7] Kefayati, G.R., *et al.*, Three-Dimensional Lattice Boltzmann Simulation on Thermosolutal Convection and Entropy Generation of Carreau-Yasuda Fluids, *International Journal of Heat and Mass Transfer, 131* (2019), pp. 346-364

[8] Turan, O., *et al.*, Laminar Natural Convection of Power-Law Fluids in a Square Enclosure Submitted from below to a Uniform Heat Flux Density, *Journal of Non-Newtonian Fluid Mechanics, 199* (2013), pp. 80-95

[9] Alloui, Z., *et al.*, Natural Convection of Carreau–Yasuda Non-Newtonian Fluids in a Vertical Cavity Heated from the Sides, *International Journal of Heat and Mass Transfer, 84* (2015), pp. 912-924

[10] Malkeson, S.P., *et al.*, Numerical Investigation of Steady State Laminar Natural Convection of Power-Law Fluids in Side-Cooled Trapezoidal Enclosures Heated from the Bottom, *Numerical Heat Transfer, Part A : Applications, 83* (2023), 7, pp. 770-789

[11] Li, S. G., *et al.*, Numerical Simulation of Heat Transfer and Entropy Generation Due to the Nanofluid Natural Convection with Viscous Dissipation in an Inclined Square Cavity, *Numerical Heat Transfer, Part A : Applications, 86* (2024), 14, pp. 4956-4986

[12] Makayssi, T., *et al.*, Natural Double-Diffusive Convection for the Carreau Shear-Thinning Fluid in a Square Cavity Submitted to Horizontal Temperature and Concentration Gradients, *Journal of Non-Newtonian Fluid Mechanics, 297* (2021), pp. 104649

[13] Cengizci, S., *et al.*, Natural Convection in Nanofluid-Filled Quadrantal Cavities under Magnetic Field : Application of the SUPS Formulation, *Numerical Heat Transfer, Part B : Fundamentals*, (2024), pp. 1-23

[14] Brooks, A. N., *et al.*, Streamline Upwind/Petrov-Galerkin Formulations for Convection Dominated Flows with Particular Emphasis on the Incompressible Navier-Stokes Equations, *Computer Methods in Applied Mechanics and Engineering, 32* (1982), 1, pp. 199-259

[15] Kim, N., *et al.*, 3-D Least-Squares Finite Element Analysis of Flows of Generalized Newtonian Fluids, *Journal of Non-Newtonian Fluid Mechanics, 266* (2019), pp. 143-159

[16] Li, S. G, *et al.*, Least Squares Finite Element Simulation of Local Transfer for a Generalized Newtonian Fluid in 2D Periodic Porous Media, *Journal of Non-Newtonian Fluid Mechanics, 316* (2023), pp. 105032

[17] González, A., *et al.*, Numerical Study of the Use of Residual- and Non-Residual-Based Stabilized VMS Formulations for Incompressible Power-Law Fluids, *Computer Methods in Applied Mechanics and Engineering, 400* (2022), pp. 115586

[18] Cengizci, S., *et al.*, Stabilized Finite Element Simulation of Natural Convection in Square Cavities Filled with Nanofluids under Various Temperature Boundary Conditions, *International Communications in Heat and Mass Transfer, 156* (2024), pp. 107655

[19] Cengizci, S., A SUPS Formulation for Simulating Unsteady Natural/Mixed Heat Convection Phenomena in Square Cavities under Intense Magnetic Forces, *The European Physical Journal Plus, 139* (2024), 8, pp. 713

[20] Wang, D. G., *et al.*, SUPG Finite Element Method Based on Penalty Function for Liddriven Cavity Flow up to Re = 27500, *Acta Mechanica Sinica, 32* (2016), pp. 54-63

[21] Li, S. G, *et al.*, Mathematical Modeling for the Local Flow of a Generalized Newtonian Fluid in 3D Porous Media, *Applied Mathematical Modelling, 105* (2022), pp. 551-565

[22] Cengizci, S., *et al.*, A Computational Study for Simulating MHD Duct Flows at High Hartmann Numbers Using a Stabilized Finite Element Formulation with Shock-Capturing, *Journal of Computational Science, 81* (2024), pp. 102381

[23] Huang, C., *et al.*, A Semi-Implicit Three-Step Method Based on SUPG Finite Element Formulation for Flow in Lid Driven Cavities with Different Geometries, *Journal of Zhejiang University-Science A, 12* (2011), 1, pp. 33-45

[24] Yu, P. X., *et al.*, Compact Computations Based on a Stream-Function–Velocity Formulation of Two-Dimensional Steady Laminar Natural Convection in a Square Cavity, *Physical Review E, 85* (2012), 3, pp. 036703

[25] Tian, Z. F, *et al.*, A Fourth-Order Compact Finite Difference Scheme for the Steady Stream Function–Vorticity Formulation of the Navier–Stokes/Boussinesq Equations, *International Journal for Numerical Methods in Fluids, 41* (2003), 5, pp. 495-518

Received: 01.06.2025.
Revised: 27.07.2025.
Accepted: 08.08.2025.